193 nm Angle-Resolved Scatterfield Microscope for Semiconductor Metrology

Yeung Joon Sohn[1,2] *, Richard Quintanilha[1], Bryan M. Barnes[1,2] and Richard M. Silver[1]
[1]National Institute of Standards and Technology, Gaithersburg, MD
[2]KT Consulting Inc., Antioch, CA

ABSTRACT

An angle-resolved scatterfield microscope (ARSM) featuring 193 nm excimer laser light was developed for measuring critical dimension (CD) and overlay of nanoscale targets as used in semiconductor metrology. The microscope is designed to have a wide and telecentric conjugate back focal plane (CBFP) and a scan module for resolving Köhler illumination in the sample plane. Angular scanning of the sample plane was achieved by linearly scanning an aperture across the 12 mm diameter CBFP, with aperture size as small as 0.4 mm for some scans. For each aperture, the sample was illuminated over a range of angles from 12° to 48°, corresponding to a numerical aperture of 0.2 to 0.74. Angle-resolved measurement results are presented for grating targets with nominal linewidths down to 50 nm.

Keywords: scatterfield microscopy, conjugate back focal plane, angle resolved, illumination.

1. INTRODUCTION

In the area of high-resolution metrology for critical dimensions (CD) down to sub-100 nanometer target dimensions, traditional lens-based methods have already confronted a resolution limitation due to the optical diffraction limit. Many alternative methods have been developed to overcome this limitation, such as scatterometry, confocal microscopy, *etc*.[1-5] Recently, scatterfield microscopy has demonstrated a potential for improving optical measurement sensitivity and performance.[3-5] Scatterfield microscopy combines scatterometry and bright-field optical microscopy, and features Köhler illumination so that an off-axis point in the back focal plane (BFP) of an objective lens makes a plane wave illuminating the sample plane at a specific angle. The intensity distribution of the back focal plane can be modified through a conjugate to the back focal plane (CBFP), allowing control of the illumination angle to generate angle-resolved images of the sample that yield image and scattered field information simultaneously. Recently, several results have been reported from scatterfield microscopes featuring angular illumination control through a scanned aperture in the CBFP.[5-8] These demonstrations establish the potential of scatterfield microscopy for semiconductor metrology in many applications. There are three aspects of this microscopy technique that can be optimized. First, the imaging resolution can be improved by using a deep ultra-violet (DUV) wavelength. Second, the illumination homogeneity in the CBFP can be improved by adopting a source scanning method instead of an aperture scanning method. Third, additional information about the target can be collected by detecting the scattered beam in both the image and the Fourier planes. To achieve all three goals, a sophisticated new optical system design was required.

We have developed an angle-resolved scatterfield microscope which was designed for one DUV wavelength, $\lambda = 193$ nm, and a sophisticated CBFP structure to exceed the limitations described above. The design at the CBFP is modular, operating in either of two modes, full-field or angle-scan mode. The full-field mode utilizes one of several aperture plates to modify the illumination beam. For example, dipole apertures, quadrupole apertures, annular apertures, polarizers, and phase plates may be inserted. The angle-scan mode features a fiber illumination set for delivering source light to the CBFP directly, making the angular illumination homogeneous and bright enough to collect the scattered light. The CBFP is designed to be telecentric so that the optical axis of the fiber may coincide with the chief rays while being scanned. In this paper we explain the design, concept, and structure of the angle-resolved scatterfield microscope, the optimization of the illumination, and results from angular scans of grating targets.

*yeungjoon.sohn@nist.gov

Instrumentation, Metrology, and Standards for Nanomanufacturing III, edited by Michael T. Postek, John A. Allgair,
Proc. of SPIE Vol. 7405, 74050R · © 2009 SPIE · CCC code: 0277-786X/09/$18 · doi: 10.1117/12.830683

Downloaded From: http://proceedings.spiedigitallibrary.org/ on 09/20/2012 Terms of Use: http://spiedl.org/terms

2. CONSTRUCTION OF A 193 NM ARSM

The tool for scatterfield microscopy for λ =193 nm is intended to allow two modes at the CBFP, yielding manipulation flexibility, telecentric optics, and two modes of imaging at the Fourier and/or the image plane. Figure 1 shows a schematic of the optical path of the tool; the detailed specifications are presented in a previous paper.[7] The source plane is imaged to the CBFP by the first lens group at 10 times magnification, then the CBFP image is transferred to the back focal plane of an objective lens. The reflected beam from the sample plane is directed either to the image plane or to the Fourier plane using a switching mirror. Data are collected at either plane using charged-coupled device (CCD) cameras. The imaging lens and Fourier imaging lens have focal lengths of 1000 mm and 500 mm, respectively. Values were selected so that the BFP image may be fully transferred to the CCD active area. Due to the catadioptric design of the objective lens, the illumination numerical aperture is limited to 0.2 through 0.74.

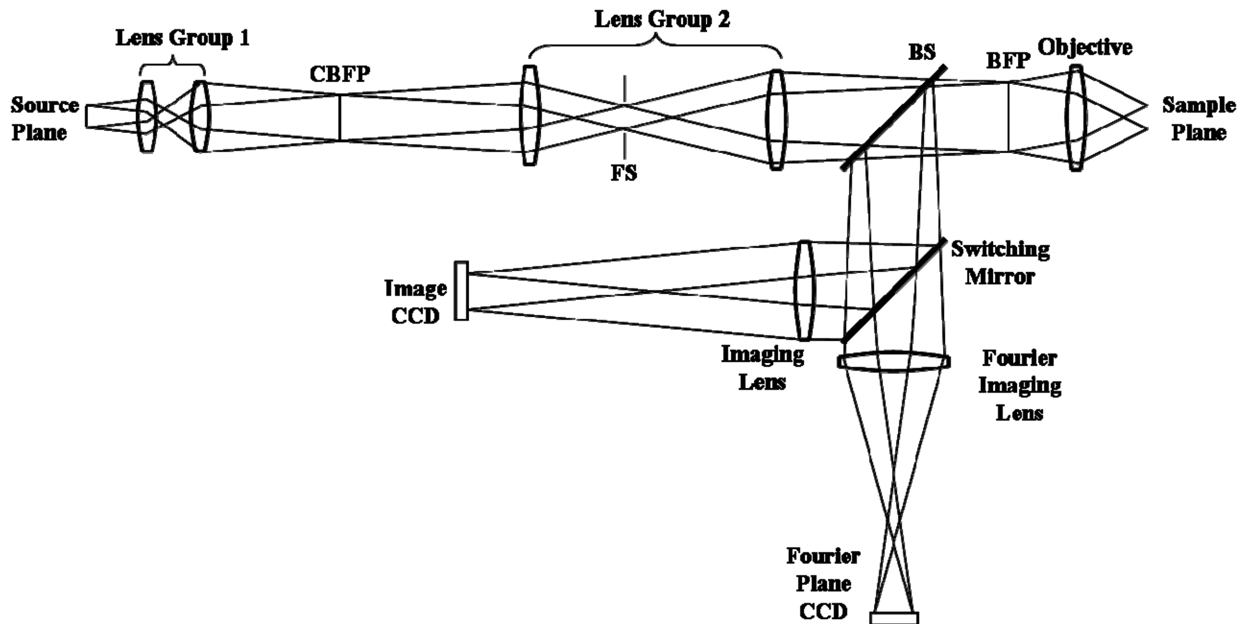

Figure 1. Schematic of the optical path of the λ =193 nm angle-resolved scatterfield microscope (ARSM). The conjugate back focal plane (CBFP) image manipulates the back focal plane (BFP) to control the angular illumination on the sample plane. The reflected beam from sample plane is imaged either into the image CCD or Fourier plane CCD by a switching mirror. The CBFP is telecentric so that scanning a beam may be possible. In the diagram, FS and BS are the field stop and beamsplitter, respectively.

If the illumination angle is controlled by scanning an aperture in the CBFP, the angular homogeneity of the illumination is affected by the irregularity of the source plane intensity. To avoid this problem, the source illumination is delivered to the CBFP via a fiber as described above. Figure 2 shows the structure of this dual mode CBFP system, with angle-scan and full-field modes. The system consists of two kinds of modules that are mounted on a linear translation stage for switching between the modes. Each module is mounted upon its own computer-controlled, motorized, three-axis stage and consists of an imaging optic or a rotating aperture holder, respectively. The full-field module is capable of holding numerous kinds of aperture shapes and the angle-scan module is capable of using phase and polarization components. The full-field module manipulates the beam coming out from the source plane when it is placed in the CBFP, while the angle-scan module manipulates the CBFP directly by using the beam delivered directly from the source via a fiber capable of transmitting 193 nm light. The size of the pinhole in the angle-scan module determines the angular width of the angular illumination beam. In this experiment two apertures, 1.2 mm and 0.4 mm in diameter, are used separately.

Downloaded From: http://proceedings.spiedigitallibrary.org/ on 09/20/2012 Terms of Use: http://spiedl.org/terms

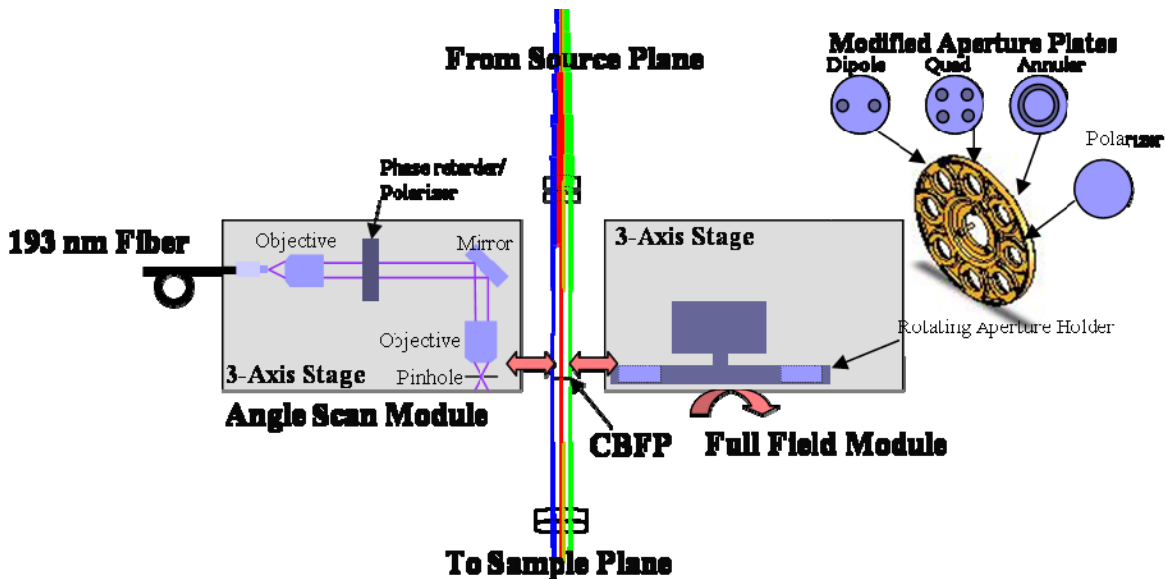

Figure 2. Schematic of two mode CBFP system. Full-field module has a rotating aperture holder which can hold eight kinds of apertures. Angle-scan module has an imaging optic that allows the image of 193 nm fiber end to be delivered directly from the light source to a pinhole and can also hold a phase or polarization element. The two modules are put on a linear translation stage, not shown.

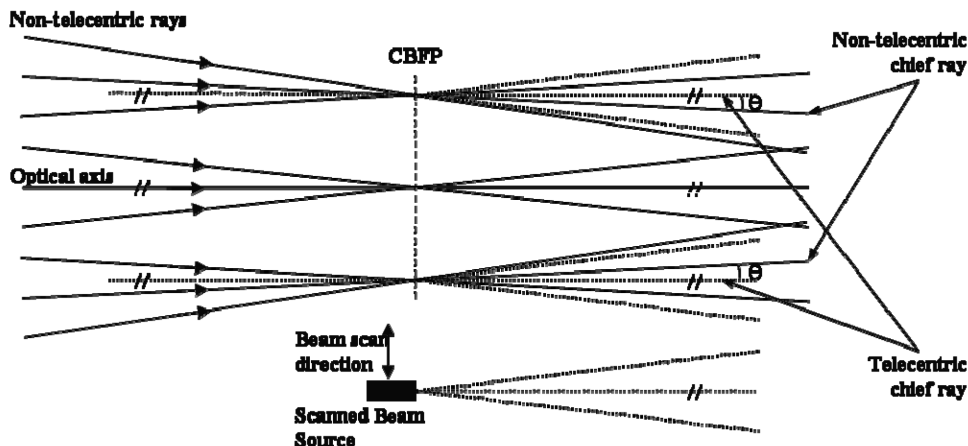

Figure 3. Schematic of possible beam paths at a CBFP with respect to telecentricity. The solid lines correspond to non-telecentric rays while the dotted lines correspond to telecentric rays. The symbol // denotes that the chief ray of the telecentric beam is always parallel to the optical axis. The 193 nm ARSM is designed to be telecentric, allowing the scanned beam source (at bottom) across the CBFP without severe optical aberrations due to the angular deviations, θ, which would arise from non-telecentricity.

In most contemporary microscopes the optics going through the objective lens is designed to be telecentric for obtaining the Köhler illumination, but the CBFP is non-telecentric because there is no need to be telecentric. In our angle-resolved scatterfield microscope the CBFP is designed to be telecentric with the chief rays going through the plane parallel to the optical axis, which permits the use of the angle-scan module. Figure 3 depicts a CBFP that has been constructed using either non-telecentric or telecentric optics. Rays are depicted as solid lines (for non-telecentic optics) and dotted lines (for telectentric optics). Some approaches to scatterfield microscopy such as an aperture scanning in CBFP do not

Downloaded From: http://proceedings.spiedigitallibrary.org/ on 09/20/2012 Terms of Use: http://spiedl.org/terms

demand telecentricity. However in our approach that uses a scanned beam source as seen above, should the source be moved off-axis then there is an angular deviation, θ, that exists if the optics are not preconfigured to be telecentric. Such a configuration results in severe aberration in both the illumination and collection paths of the microscope. The illumination angle in the sample plane would differ from the intended illumination scheme. Therefore, the design of the $\lambda = 193$ nm angle-resolved scatterfield microscope was made telecentric to allow for scanning of the source in the CBPF.

3. MICROSCOPE CHARACTERIZATION

In this section, the 193 nm angle-resolved scatterfield microscope (ARSM) is characterized in both full-field and angle-scan modes. The optical properties of the microscope are evaluated and its capabilities for performing angular scans are examined. Using the full-field optical alignment, the tool-induced shift (TIS) is measured. The TIS value is one commonly used metric for measuring the inherent tool-limited measurement accuracy. For the angle-scan mode, aperture scanning is performed for several grating targets and sensitivity to pitch and linewidth is demonstrated.

3.1 Full-Field Mode, Detected at the Image Plane

Frame-in-frame type overlay targets with the inside trench and outside protrusion from an Overlay Metrology Advisory Group (OMAG) 4 wafer were used for TIS measurements as shown in Figure 4 (a). Both square frames have line width of 1 µm, trench depth and protrusion height of 0.6 µm, and frame width and height of 15 µm and 7 µm, respectively. The horizontal and vertical TIS values are quantified by measuring the target at 0° and 180° angles of rotation with respect to the microscope.[9] The TIS values were calculated using

$$TIS_x = \frac{X_{0^\circ} + X_{180^\circ}}{2}, \ \ and \qquad (1)$$
$$TIS_x = \frac{Y_{0^\circ} + Y_{180^\circ}}{2},$$

where X_α and Y_α are the overlay offsets for a particular rotation angle α. Overlay offset arises from the misalignment of one photolithographic layer with respect to a prior layer. In general, the lower the magnitude of the TIS value, the better performance of the tool; the rotation inherent in TIS minimizes the effects of the overlay target leaving the instrument as the primary source for TIS.

Overlay offsets are determined using averaged line profiles through the center of the target. Figures 4 (b) and (c) are the line intensity profiles of the captured target image, where the *x* and *y* axes of the graphs are in units of pixel and arbitrary intensity, and the pixel pitch corresponds to 71 nm. When capturing the target image for measurement, the focus is important because the inside frame is a trench and the outside frame, a protrusion. For this measurement we focused on the wafer surface, the intermediate point between the trench and protrusion. The target profile asymmetry is affected by the asymmetry in angular illumination and it is controlled by the CBFP aperture position. When the target is centered in the sampling area, the scattering interference intensity from the lines is adjusted to be symmetric by moving the full-field module in both the horizontal and vertical direction. High-resolution images and line profiles for two different targets were measured at 0° and 180°, with three iterations per target.

Table 1. Measured TIS values

	TIS Value (nm)	
	Horizontal	Vertical
Target 1	-1.47	-0.28
Target 2	-3.64	2.22

Downloaded From: http://proceedings.spiedigitallibrary.org/ on 09/20/2012 Terms of Use: http://spiedl.org/terms

The averaged TIS value from the three measurements for each target is shown in Table 1. For both targets the vertical TIS values appear to be better than the horizontal values. We assume that this discrepancy at the time was the result of misalignment of optics and/or aperture position along the horizontal axis. These TIS values are the initial measurements for this instrument, and TIS has not yet been optimized to the sub-nm regime. Such optimization will be impeded by the relatively high numerical aperture (NA=0.74) of the objective lens and the deep ultra-violet wavelength of the instrument. A short wavelength leads to a small depth-of-focus, which combined with the high NA will lead to large TIS values. Nevertheless, this initial measurement is promising, as the smallest of these four stated TIS values is $< \lambda/100$, which would be acceptable for the tool.

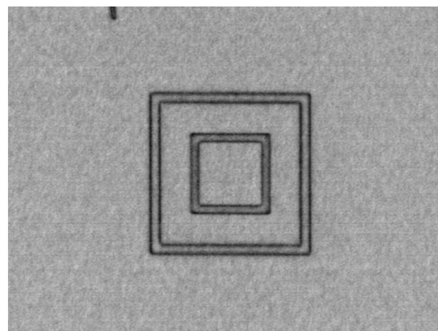

(a) Picture of overlay target for TIS measurement

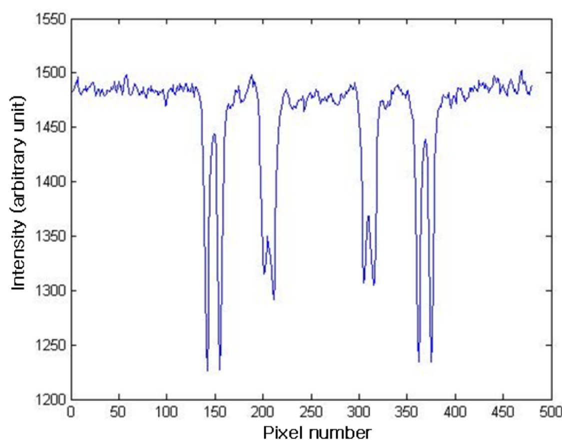

(b) Intensity profile for horizontal axis

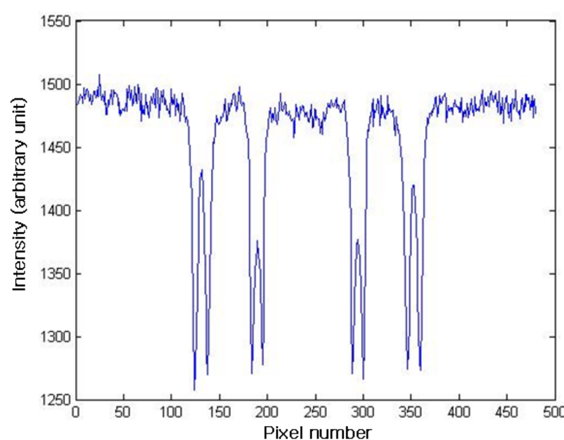

(c) Intensity profile for vertical axis

Figure 4. High-resolution image and line intensity profiles of a frame-in-frame target. Dimensions of the overlay target in (a) are 1 μm in line width, 0.6 μm in line depth and height, 15 μm and 7 μm in box width and height, respectively. The frame is measured at 0° and 180° rotations with respect to the microscope three times. In (b) and (c), the horizontal and vertical axes are in units of pixel and arbitrary intensity, respectively, and the pixel pitch corresponds to 71 nm.

One application for full-field imaging is the measurement of new types of overlay targets that are smaller in area than those used presently. Several such targets can be placed within the field-of-view of the tool. Overlay measurement may also be enhanced from high-magnification imaging coupled with the angle-scan mode. As a demonstration of the advantages of the angle-scan mode, measurements have been performed on arrays of individually unresolved lines as imaged at the Fourier plane.

3.2 Angle-Scan Mode, Detected in Fourier Plane

When an aperture of the angle-scan module moves along the CBFP to control the illumination angle, as shown in Figure 2, the relationship of the linear position, D, in CBFP to the illumination angle, θ, may be expressed as

Downloaded From: http://proceedings.spiedigitallibrary.org/ on 09/20/2012 Terms of Use: http://spiedl.org/terms

$$\theta = \arcsin \frac{1}{\sqrt{(\kappa / D)^2 + 1}}, \tag{2}$$

where, $\kappa^2 = D^2(1/NA^2 - 1)$ is a constant for the numerical aperture, NA, of the objective lens. Its value can be determined if both the illumination angle at the sample plane and the position of the center of the scanning beam in CBFP are known. In this experiment, this value is determined by the maximum illumination angle and the marginal beam position of CBFP.

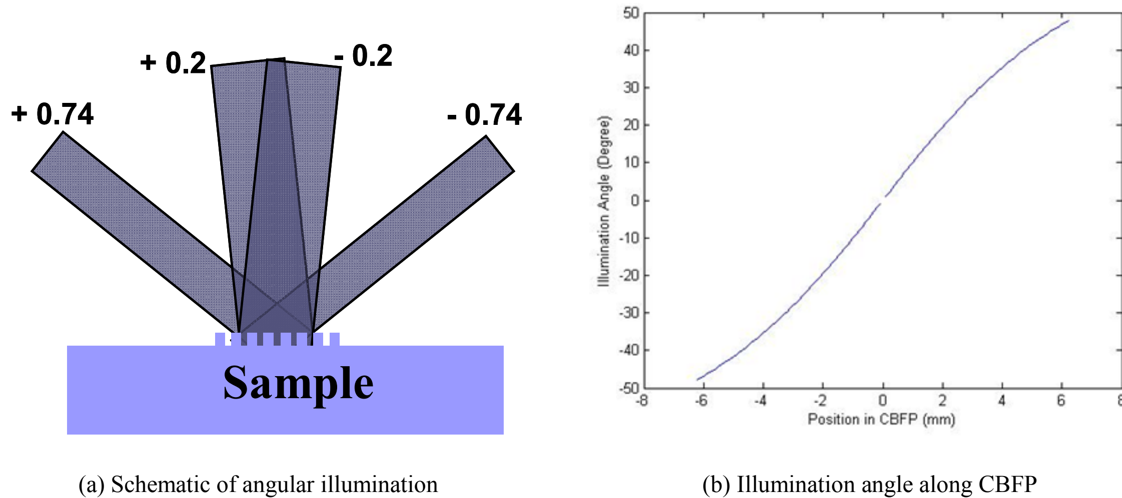

(a) Schematic of angular illumination

(b) Illumination angle along CBFP

Figure 6. Angular illumination on grating target. (a) A schematic of angular illumination showing NA 0.2 to 0.74 which corresponds to 12° to 48°. (b) The calculated variations of the illumination angle along the position in CBFP, respectively.

As shown in Figure 6 (a) the illumination angle is ± 0.2 NA through ± 0.74 NA which corresponds to 12° through 48°, but the actual illumination angle is less than the nominal illumination angle of the objective lens due to the finite illumination beam size. Illumination beams from apertures 1.2 mm and 0.4 mm in diameter were used, with the resultant illumination beams having an angular width between 6.2° and 10.9° (for the 1.2 mm diameter) and between 1.9° and 3.8° (for 0.4 mm diameter).

Figure 7 shows Fourier-plane images of the beams reflected from two grating samples of 100 nm linewidth with 300 nm period (left) and 50 nm linewidths with 250 nm period (right) by scanning two apertures of 1.2 mm (left) and 0.4 mm (right) in CBFP. The upper two are the images of the diffracted 0th and 1st order beams showing that the 1st order beam reflected from the denser grating has a higher diffraction angle than the less dense grating, as expected. The lower two pictures are the overlapped images of 0th order reflected beams showing that illumination at higher angles leads to lower reflectivity than at lower angles for the unpolarized illumination beam.

The intensity variations of the zero-order beam for the line grating of 100 nm linewidth, 300 nm pitch and bare silicon was measured along the illumination angle by scanning an aperture of 1.2 mm diameter in the CBFP with results shown in Figure 8 (a). There is almost no variation in intensity as a function of illumination angle for the bare silicon, as expected for unpolarized light. For the line grating, the intensity decreases as the incident angle increases, as expected from diffraction theory for this line grating. Figure 8 (b) shows the results from scanning a beam 0.4 mm in diameter and measuring the intensity of the zero-order beam reflected by two line gratings. One grating has a linewidth of 50 nm with a pitch of 250 nm, while the other features a linewidth of 80 nm with a pitch of 400 nm. The optical response from the two gratings is substantially different; the denser grating yields a lower signal, demonstrating a capability to differentiate between the two gratings. This example illustrates the potential for identifying variations between line gratings of nanoscale gratings with a sensitivity of much less than 30 nm.

Downloaded From: http://proceedings.spiedigitallibrary.org/ on 09/20/2012 Terms of Use: http://spiedl.org/terms

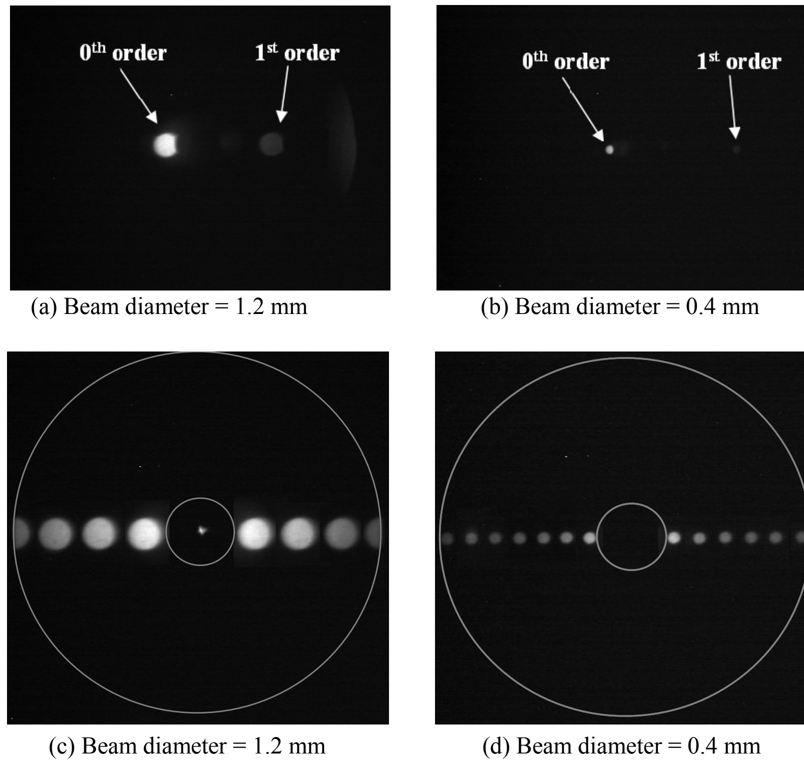

(a) Beam diameter = 1.2 mm (b) Beam diameter = 0.4 mm

(c) Beam diameter = 1.2 mm (d) Beam diameter = 0.4 mm

Figure 7. Pictures of images in the Fourier plane for two kinds of aperture size of the CBFP. (a), (c) are beams reflected from a grating of 100 nm linewidth, 300 nm period by scanning a beam size of 1.2 mm diameter and (b), (d) from a grating of 50 nm linewidth, 250 nm period by a beam size of 0.4 mm diameter. The above two pictures shows 0th, 1st order beam and the below two the overlapped 0th order beams along the illumination angle.

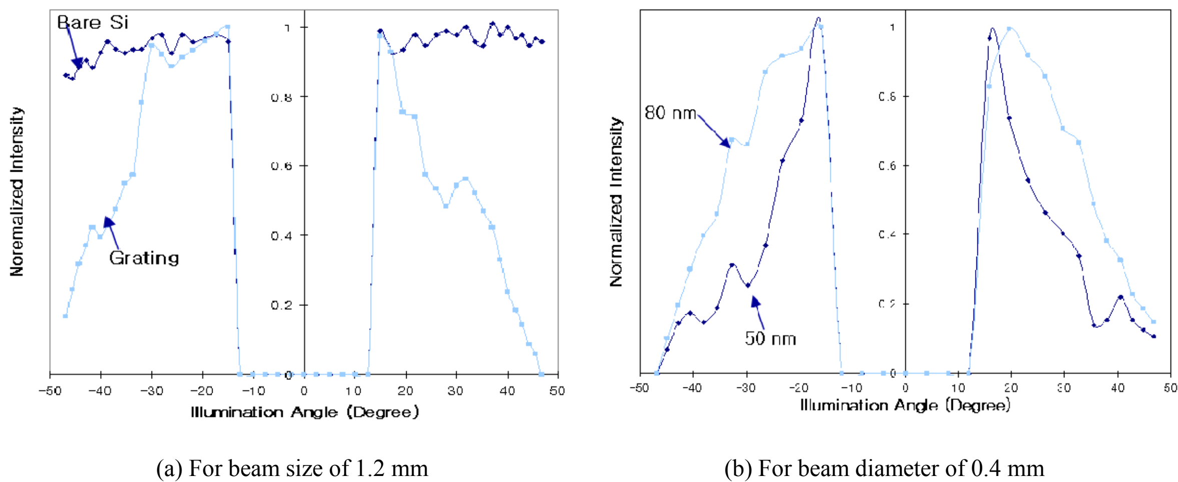

(a) For beam size of 1.2 mm (b) For beam diameter of 0.4 mm

Figure 8. Normalized intensity variation of zero-order scattered beam. (a) Bare silicon and a grating target of 100 nm linewidth, 300 nm period by scanning a beam of 1.2 mm diameter. (b) Two line gratings with 50 nm linewidth, 250 nm period and 80 nm linewidth, 400 nm period by scanning a beam of 0.4 mm diameter. The scanning steps of the apertures are 0.2 mm and 0.5 mm for (a), (b) respectively. Incident beam was unpolarized.

Downloaded From: http://proceedings.spiedigitallibrary.org/ on 09/20/2012 Terms of Use: http://spiedl.org/terms

4. SUMMARY

An angle-resolved scatterfield microscope (ARSM) was developed for high-resolution optical metrology, operating with λ = 193 nm light from an ArF excimer laser. The ARSM featured full-field and angle-scan modes, due to its telecentric configuration. High-resolution imaging was demonstrated at 193 nm and the tool demonstrated an acceptable TIS value for such an initial test. Homogeneous angular illumination was obtained using a 193 nm fiber as the source for the conjugate back focal plane (CBFP) and the tool was characterized with respect to angular illumination for analyzing dense line gratings down to nominal linewidths of 50 nm. The potential of scatterfield microscopy was again demonstrated, showing high sensitivity to variation in the line profiles by using scanned angular illumination. Future work will include polarization control, several applications in defect metrology, and nanoscale dimensional metrology.

5. ACKNOLWEDGEMENTS

The authors wish to thank Dilip Patel, Pete Lipscomb, and Milton Godwin from International SEMATECH, ISMI for patterned defect wafers and measurement support. The authors are grateful for financial support from ISMI, the Office of Microelectronics Programs at NIST and the Scatterfield Optical Competence also from NIST.

REFERENCES

1. K. P. Bishop, S. M. Gaspar, L. M. Milner, S. Sohail, H. Naqvi and J. R. McNeil, "Grating line shape characterization using scatterometry," Proc. SPIE **1545**, 64 (1991).
2. R. Attota, Richard Silver, and B. M. Barnes, "Optical through-focus technique that differentiates small changes in line width, line height and sidewall angle for CD, overlay, and defect metrology applications," Proc. SPIE **6922**, 6922E-1 (2008).
3. H. J. Patrick, R. Attota, B. M. Barnes, T. A. Germer, M. T. Stocker, R. M. Silver, M. R. Bishop, "Scatterfield microscopy using back focal plane imaging with an engineered illumination field," Proc. SPIE **6152**, 61520J (2006).
4. Heather J. Patrick, Ravikiran Attota, Bryan M. Barnes, Thomas A. Germer, Ronald G. Dixson, Michael T. Stocker, Richard M. Silver, and Michael R. Bishop, "Optical critical dimension measurement of silicon grating targets using back focal plane scatterfield microscopy," J. Micro/Nanolith. MEMS MOEMS **7**, 013012 (2008).
5. R. M. Silver, B. M. Barnes, A. Heckert, R. Attota, R. Dixson and J. Jun, "Angle resolved optical metrology," Proc. SPIE **6922**, 69221M (2008).
6. Y. J. Sohn, Richard M. Silver, "Kohler illumination analysis for high-resolution optical metrology using 193 nm light," Proc. SPIE **6518**, 65184V (2007).
7. Y. J. Sohn, R. Quintanilha, Lowell Howard, and R. M. Silver, "Analysis of Köhler illumination for 193 nm scatterfield microscope," Proc. SPIE **7272**, 72723T (2009).
8. R. Quintanilha, Y. Sohn, B. M. Barnes, L. Howard, and R. Silver "Critical dimension measurements using a 193 nm scatterfield microscope," Proc. SPIE **7390**, 73900S (2009).
9. P. Rai-Choudhury, [Handbook of microlithography, micromachining, and microfabrication], Bellinghan & Washington, 500-515 (1997).
10. R. Attota, M. Stocker, R. Silver, A. Heckert, H. Zhou, R. Kasica, L. Chen, R. Dixson, G. Orji, B. Barnes and P. Lipscomb, "Through-focus scanning and scatterfield optical methods for advanced overlay targets analysis," Proc. SPIE **7272**, 727214 (2009).

Downloaded From: http://proceedings.spiedigitallibrary.org/ on 09/20/2012 Terms of Use: http://spiedl.org/terms